Design of Antithrombotic PVA-Based Electrospun Surfaces for Small-Diameter Vascular Grafts

JANSET ÖZTEMUR, SUZAN ÖZDEMİR, HANDE SEZGİN, İPEK YALÇIN-ENİŞ
Textile Engineering
Istanbul Technical University
Beyoglu, Istanbul
TÜRKIYE

Abstract: - Although substantial progress has been made in the design of biomaterial-based electrospun tissue-engineered scaffolds, thrombosis continues to limit the performance of small-diameter vascular grafts. In response to this challenge, increasing attention has been directed toward graft designs that incorporate antithrombotic functionality to enhance hemocompatibility. In the current study, poly(vinyl alcohol) (PVA) based electrospun surfaces were developed to address thrombosis-related problems in vascular graft applications, and the incorporation of enoxaparin and fondaparinux was examined as an antithrombotic approach. In this context, PVA solutions were prepared at 6 wt%, and the effect of drug incorporation on surface characteristics was assessed by measuring fiber diameter, pore size, and overall porosity. The resulting electrospun structures displayed fiber diameters of 187-239 nm and porosity exceeding 86%, a range generally regarded as advantageous for cellular infiltration. On the other hand, the incorporation of enoxaparin resulted in pronounced changes in fiber diameter and porosity. In addition, water contact angle measurements demonstrated that both neat and drug-loaded PVA surfaces retained a hydrophilic character, supporting their suitability for cell adhesion. The presence of enoxaparin and fondaparinux on the fibrous surfaces was further confirmed by FTIR analysis, demonstrating the successful integration of the antithrombotic agents.

Key-Words: - biomaterials, PVA, tissue-engineering, vascular graft, antithrombotic drug, thrombosis, electrospinning

Received: January 22, 2026. Revised: April 13, 2026. Accepted: June 5, 2026. Published: August 17, 2026.

1 Introduction

Small-diameter vascular grafts remain limited by a high risk of early thrombosis, which arises immediately after implantation due to direct blood contact with artificial surfaces lacking an endothelial lining. Rapid adsorption of plasma proteins, including fibrinogen and von Willebrand factor, promotes platelet adhesion and activation, triggering the coagulation cascade and ultimately compromising graft patency [1], [2]. To mitigate this issue, synthetic grafts, particularly clinically used materials such as expanded polytetrafluoroethylene (ePTFE), are frequently combined with systemic antithrombotic therapy. Although these grafts provide high mechanical stability, their intrinsic thrombogenicity in small-diameter applications necessitates adjunct anticoagulation. Clinical and preclinical studies indicate that post-operative anticoagulant administration can support short-term patency in ePTFE-based grafts; however, this strategy relies on systemic drug exposure and does not directly address thrombogenic interactions at the graft surface [3], [4]. Although antithrombotic agents are effective drugs, systemic administration is associated with bleeding risks; therefore, localized strategies targeting the blood-material interface are increasingly preferred. In this context, unfractionated heparin (UFH) has been widely studied due to its strong anticoagulant activity and high biocompatibility [5], [6], [7]. However, the use of UFH is limited due to its short half-life and animal origin [8]. Accordingly, low molecular weight heparins (LMWHs), such as enoxaparin, offer improved pharmacokinetics and more predictable anticoagulant responses [9], [10], while also exhibiting anti-inflammatory and antifibrotic effects that may support vascular healing [11], [12]. Enoxaparin enhances antithrombin III-mediated inhibition of factor Xa, thereby suppressing platelet activation [13]. Nevertheless, its direct incorporation into vascular grafts remains limited, with rapid drug release frequently reported [14]. Similarly, fondaparinux, a synthetic factor Xa inhibitor, presents a lower risk of heparin-induced thrombocytopenia due to its reduced affinity for platelet factor 4 [15], [16]; however, despite its widespread systemic use with both biodegradable and non-biodegradable grafts [3],

its integration into graft architectures has not been investigated.

UFH, LMWHs, and synthetic anticoagulants share a critical limitation; short half-lives and rapid clearance following systemic administration, which restrict sustained therapeutic efficacy at the graft-blood interface [17]. In addition, physical adsorption strategies provide only transient drug presence and are therefore insufficient for long-term thrombosis prevention. Accordingly, there is a clear need for localized delivery systems capable of maintaining antithrombotic activity directly on graft surfaces. In this regard, electrospinning has emerged as a versatile fabrication technique that enables the production of extracellular matrix-mimicking fibrous architectures while allowing the direct incorporation of anticoagulant agents into the polymer matrix. Compared with conventional surface modification or systemic administration approaches, electrospun systems offer greater control over drug distribution and release kinetics, thereby providing a promising platform for prolonging antithrombotic efficacy, enhancing hemocompatibility, and improving the long-term patency of small-diameter vascular grafts [18].

The aim of this study is to develop electrospun polymeric vascular graft surfaces incorporating enoxaparin and fondaparinux as localized antithrombotic agents and to evaluate their effects on hemocompatibility and drug release behavior. By addressing the limitations of systemic anticoagulation and rapid drug release, this study aims to inform the design of vascular grafts with improved resistance to early thrombosis and enhanced long-term performance.

2 Materials and Methods

2.1 Materials

PVA (Sigma-Aldrich) with a molecular weight range of 146,000-186,000 g/mol and a degree of hydrolysis exceeding 87-89% was utilized. Distilled water served as the solvent for all polymer solutions. Enoxaparin sodium (Oksapar®, 6000 anti-Xa IU/0.6 mL; Koçak Farma) and fondaparinux (Arixtra®, 2.5 mg/0.5 mL; Eczacıbaşı) were selected as the antithrombotic agent and were used in a commercially available formulation.

2.1 Methods

Solution Preparation

The polymer concentration was set at 6%, and PVA was added incrementally to deionized water under continuous magnetic stirring, followed by heating at 85-90 °C for approximately 2 h to ensure complete polymer dissolution and solution homogeneity. The solution was then allowed to cool to ambient temperature. Subsequently, enoxaparin sodium/fondaparinux was incorporated into a commercially available aqueous formulation. One full injection was added to 10 g of polymer solution, and the mixtures were gently stirred at 100 rpm to achieve uniform drug distribution throughout the polymer solution. Furthermore, drug incorporation was performed after cooling to minimize the risk of thermal degradation, and the final drug content was adjusted to meet clinically recommended dosing guidelines.

Surface Fabrication

Electrospinning was performed using a closed-chamber vertical electrospinning system (Nanospinner NE100+, Inovenso, Türkiye) equipped with a rotating cylindrical collector to fabricate tubular scaffolds. The collector rotation speed was maintained at 200 rpm to obtain randomly oriented fibrous structures, selected to mimic the morphological characteristics of the tunica intima (the inner layer of the native artery). During electrospinning, ambient temperature and relative humidity were controlled at 13 ± 3 °C and 60 ± 5%, respectively. The corresponding electrospinning parameters and sample codes are provided in Table 1.

Table 1. Sample codes and production parameters for neat PVA and drug-loaded PVA surfaces

Sample Code	Polymer System	Incorporated Drug	Applied Voltage (kV)	Flow Rate (mL/h)	Tip-to-Collector Distance (cm)
PVA6	PVA	-	22	0.9	15
PVA6_E	PVA	enoxaparin	17.5	0.5	17
PVA6_F	PVA	fondaparinux	18	0.6	15

Morphological Analysis

The surface morphology of the electrospun surfaces was characterized using a scanning electron microscope (SEM; Zeiss Evo MA10). All samples were coated with a gold-palladium (Au-Pd) alloy (Quorum SC7620) prior to imaging, to improve surface conductivity. SEM images were acquired at a magnification of 10kx. Quantitative analyses of fiber diameter, pore area, and porosity were performed using ImageJ. For each sample, at least 50 fibers were

randomly selected and measured, and the results are reported as mean ± standard deviation. Also, porosity and pore area were determined from SEM micrographs using an ImageJ-based thresholding method.

Hydrophilicity Analysis

The wettability of the fabricated scaffolds was assessed by water contact angle (WCA) measurements using the sessile drop method with a KSV extension optical contact angle meter.

Fourier-Transform Infrared (FTIR) Spectroscopy Analysis

Fourier-transform infrared (FTIR) spectroscopy was utilized to characterize the chemical structure of the electrospun surfaces and to verify the presence of both polymeric constituents and incorporated antithrombotic agents. Spectral measurements were performed using a UATR Two spectrometer (PerkinElmer) operating in attenuated total reflectance (ATR) mode over the wavenumber range of 4000-400 cm^{-1}.

Statistical Analysis

Statistical analysis was conducted to assess differences between neat and drug-loaded electrospun surfaces. Independent sample t-tests were used, with 50 measurements collected per sample.

3 Results and Discussion

3.1 Morphological Analysis

To evaluate the morphological characteristics of the electrospun surfaces, SEM was employed. Figure 1a, 1b, and 1c show representative SEM micrographs of neat PVA and drug-loaded PVA electrospun surfaces. Overall, continuous and relatively uniform fibrous morphologies were obtained for the PVA6, PVA6_E, and PVA6_F samples. While occasional bead formation was observed in the PVA6_E surface (Figure 1b), the presence of extensive fibrous regions suggests that homogeneous fiber formation can still be achieved through appropriate control of solution preparation and electrospinning parameters.

Moreover, fiber diameter analysis indicated that all samples predominantly exhibited fiber diameters within the range of 187-239 nm (Table 2). Incorporation of enoxaparin led to a reduction in fiber diameter compared to the neat PVA surface, with the average fiber diameter decreasing from 227 nm for PVA6 to 187 nm for PVA6_E. However, incorporation of fondaparinux in the present study did not lead to a pronounced change in fiber diameter, suggesting a drug-specific influence on solution properties and fiber formation behavior. Although studies investigating the incorporation of enoxaparin and fondaparinux into electrospun fibers remain limited, similar diameter reduction trends have been reported for heparin-containing PVA-based systems. Orozco et al. (2025) observed a decrease in fiber diameter from approximately 131.08 nm to 114.5 nm as the heparin content increased from 5% to 20% in uncrosslinked PVA-gelatin electrospun matrices [19]. Moreover, the enoxaparin-loaded surface exhibited a significant decrease compared to neat PVA ($p<0.05$), while no statistically significant difference was detected between neat PVA and the fondaparinux-loaded surface ($p>0.05$).

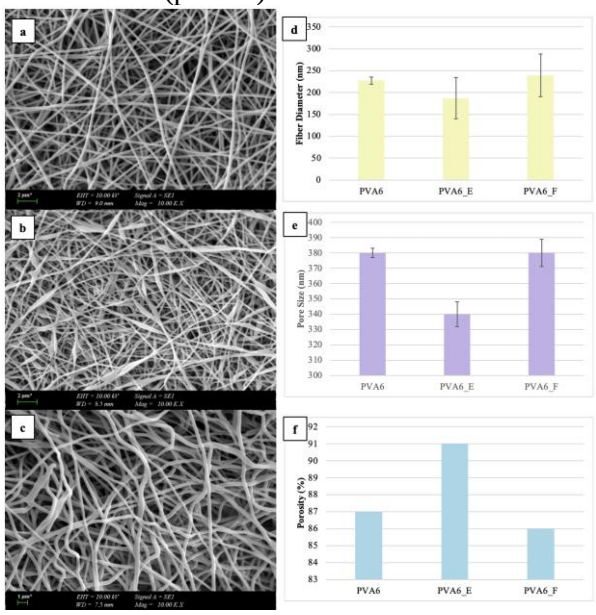

Fig. 1: SEM micrographs of (a) PVA6, (b) PVA6_E, and (c) PVA6_F, along with quantitative analysis of (d) fiber diameter, (e) pore size, and (f) porosity

On the other hand, fiber diameter is closely related to pore size and overall porosity, with larger fiber diameters generally associated with larger pores and reduced porosity [20], [21]. Consistent with this relationship, the PVA6_E sample exhibits the smallest average fiber diameter, the highest porosity (91%), and the smallest pore size (340 nm). Furthermore, pore size analysis indicated a significant reduction in pore size for enoxaparin-loaded fibers ($p<0.05$), whereas fondaparinux-loaded surfaces exhibited pore sizes similar to those of control PVA fibers ($p>0.05$). These findings indicate that enoxaparin incorporation influences not only fiber morphology but also the microstructural organization of the electrospun network, which may be relevant for cell activities on the scaffold surface.

3.2 Hydrophilicity Analysis

Figure 2 presents the water contact angle measurements together with representative droplet images of the samples. Contact angle analysis was employed to assess surface wettability, which is governed by both surface chemistry and microstructural features. The neat PVA surface exhibited a low contact angle of 58.7 ± 1.51°, consistent with its intrinsic hydrophilicity. This value serves as a reference for evaluating the influence of antithrombotic drug incorporation and surface design strategies [22], [23].

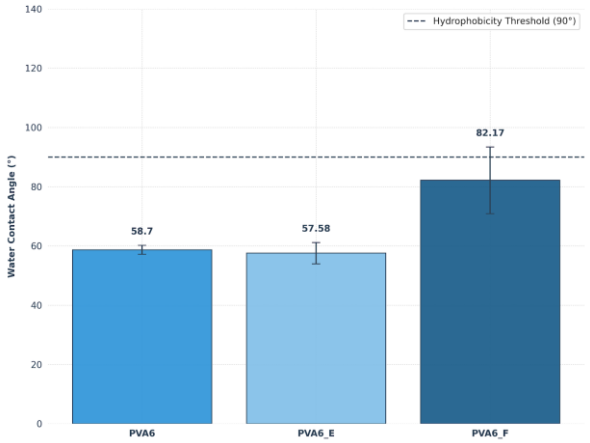

Fig. 2: Water contact angle values of the samples

The effect of drug incorporation on wettability depended on the type of antithrombotic agent. The enoxaparin-loaded PVA sample exhibited contact angle values comparable to neat PVA (57.58±3.60°), indicating that enoxaparin did not diminish the intrinsic hydrophilicity of the PVA matrix. Given enoxaparin's polar nature, this behavior suggests that the drug helps maintain water affinity at the surface. Similar effects have been reported for heparin-modified PVA surfaces, in which increased hydrophilicity was attributed to the presence of polar functional groups [24]. However, PVA surfaces containing fondaparinux exhibited higher contact angles (82.17±11.23°), suggesting less influence on surface wettability.

3.2 FTIR Analysis

As illustrated in Figure 3, the FTIR spectrum of neat PVA is characterized by a broad absorption band between 3300 and 3400 cm^{-1}, which is attributed to O-H stretching vibrations and reflects the intrinsic hydrophilicity of the polymer. This hydroxyl-related band remains evident in both PVA6_E and PVA_F samples, consistent with the presence of hydroxyl- and sulfate-rich antithrombotic agents within the fibrous matrix. The increased broadness of this region suggests the formation of additional hydrogen-bonding interactions arising from drug incorporation [25].

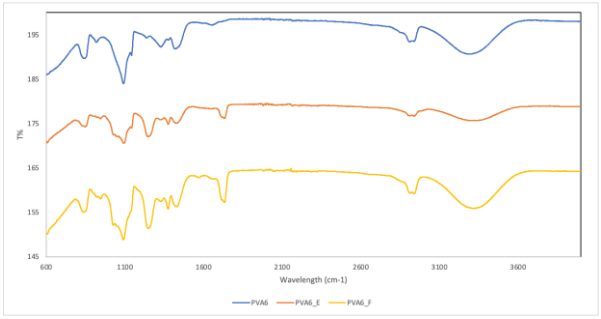

Fig. 3: FTIR analysis of the samples

Characteristic absorption peaks associated with the PVA backbone were also observed, including C-H stretching vibrations around 2900 cm^{-1}, CH_2 bending modes near 1445 cm^{-1}, C-O stretching of secondary alcohol groups at approximately 1090 cm^{-1}, and skeletal C-C vibrations at around 845 cm^{-1} [26]. In addition, weak bands detected in the 1600-1650 cm^{-1} region were assigned to protonated amine vibrations, while absorption bands between 1200 and 1250 cm^{-1} corresponded to sulfate (S=O) stretching modes [27], [28]. The presence of these characteristic features in both enoxaparin- and fondaparinux-loaded PVA samples confirms the successful incorporation of the antithrombotic agents into the PVA-based electrospun surfaces.

4 Conclusion

In this study, PVA-based electrospun surfaces incorporating enoxaparin and fondaparinux were developed to address thrombosis-related limitations in small-diameter vascular graft applications. The electrospun structures exhibited fiber diameters in the nanometer range and high porosity exceeding 86%, features considered favorable for cellular infiltration and tissue integration. Despite these morphological changes, all surfaces retained a hydrophilic character, as confirmed by water contact angle measurements, supporting their potential suitability for cell adhesion and hemocompatible performance. FTIR analysis further verified the successful integration of both enoxaparin and fondaparinux into the fibrous matrices. The findings demonstrate that antithrombotic drugs can be incorporated into PVA-based electrospun scaffolds without compromising key structural and surface properties, highlighting their potential as hemocompatible surface designs for vascular graft applications.

Acknowledgement
This study is supported by the TUSEB Project under grant no. 46602, and ITU Scientific Research Projects Unit, project number MDK-2025-46820.

References:

[1] Naegeli, K. M., Kural, M. H., Li, Y., Wang, J., Hugentobler, E. A., & Niklason, L. E. (2022). Bioengineering Human Tissues and the Future of Vascular Replacement. Circulation Research, 131(1), 109-126. https://doi.org/10.1161/CIRCRESAHA.121.319984

[2] Norouzi, S. K., & Shamloo, A. (2019). Bilayered heparinized vascular graft fabricated by combining electrospinning and freeze drying methods. Materials Science and Engineering C, 94, 1067-1076. https://doi.org/10.1016/j.msec.2018.10.016

[3] Durairaj, M. S., Mathew, J. S., Mallick, S., Nair, K., Manikandan, K., Varghese, C. T., Chandran, B., Amma, B. S. P. T., Balakrishnan, D., Gopalakrishnan, U., Menon, R. N., Vayoth, S. O., & Surendran, S. (2021). Middle hepatic vein reconstruction in adult living donor liver transplantation: a randomized clinical trial. British Journal of Surgery, 108(12), 1426-1432. https://doi.org/10.1093/bjs/znab346

[4] El Hennawy, H. M., Al Atta, E., Awadh, A., Safar, O., Al Kawasmeh, S., Mansour, Y. S., Zaitoun, M. F., & Al Faifi, A. S. (2024). Successful Vascular Graft Reconstruction of Short Renal Artery Using Polytetrafluoroethylene (PTFE) in Living Donor Kidney Transplantation—A Case Report and Review of Literature. Transplantation Proceedings, 1-5. https://doi.org/10.1016/j.transproceed.2024.11.013

[5] Ye, L., Wu, X., Duan, H. Y., Geng, X., Chen, B., Gu, Y. Q., Zhang, A. Y., Zhang, J., & Feng, Z. G. (2012). The in vitro and in vivo biocompatibility evaluation of heparin-poly(ε-caprolactone) conjugate for vascular tissue engineering scaffolds. Journal of Biomedical Materials Research - Part A, 100 A(12), 3251-3258. https://doi.org/10.1002/jbm.a.34270

[6] Saravanababu, M., Jin, X., & Linhardt, R. J. (2013). Immobilization of Heparin: Approaches and Applications Saravanababu. Journal of Chemical Information and Modeling, 53(9), 1689-1699.

[7] Cheng, C., Sun, S., & Zhao, C. (2014). Progress in heparin and heparin-like/mimicking polymer-functionalized biomedical membranes. Journal of Materials Chemistry B, 2(44), 7649-7672. https://doi.org/10.1039/c4tb01390e

[8] Erginer, M., Akcay, A., Coskunkan, B., Morova, T., Rende, D., Bucak, S., Baysal, N., Ozisik, R., Eroglu, M. S., Agirbasli, M., & Toksoy Oner, E. (2016). Sulfated levan from Halomonas smyrnensis as a bioactive, heparin-mimetic glycan for cardiac tissue engineering applications. Carbohydrate Polymers, 149, 289-296. https://doi.org/10.1016/j.carbpol.2016.04.092

[9] Aslani, S., Kabiri, M., Kehtari, M., & Hanaee-Ahvaz, H. (2019). Vascular tissue engineering: Fabrication and characterization of acetylsalicylic acid-loaded electrospun scaffolds coated with amniotic membrane lysate. Journal of Cellular Physiology, 234(9), 16080-16096. https://doi.org/10.1002/jcp.28266

[10] Oduah, E. I., Linhardt, R. J., & Sharfstein, S. T. (2016). Heparin: Past, present, and future. Pharmaceuticals, 9(3), 1-12. https://doi.org/10.3390/ph9030038

[11] Singh, C., Wong, C., & Wang, X. (2015). Medical Textiles as Vascular Implants and Their Success to Mimic Natural Arteries. Journal of Functional Biomaterials, 6(3), 500-525. https://doi.org/10.3390/jfb6030500

[12] Yang, X., Wang, Q., Zhang, A., Shao, X., Liu, T., Tang, B., & Fang, G. (2022). Strategies for sustained release of heparin: A review. Carbohydrate Polymers, 294(April), 119793. https://doi.org/10.1016/j.carbpol.2022.119793

[13] Elliott, M. B., Matsushita, H., Shen, J., Yi, J., Inoue, T., Brady, T., Santhanam, L., Mao, H. Q., Hibino, N., & Gerecht, S. (2022). Off-the-shelf, heparinized small diameter vascular graft limits acute thrombogenicity in a porcine model. Acta Biomaterialia, 151, 134-147. https://doi.org/10.1016/j.actbio.2022.07.061

[14] Zendedel, E., Javdani, M., Ebrahimi-Barough, S., Ai, J., Jaafari, M. R., Mirzaei, S. A., Soleimannejad, M., Askari, V. R., & Asadpour, S. (2024). Development of small-diameter vascular grafts using PCL/PLA/gelatin/PVA/hyaluronic acid nanofibers containing VEGF/enoxaparin. Journal of Drug Delivery Science and

Technology, 101(PA), 106171. https://doi.org/10.1016/j.jddst.2024.106171

[15] Cai, Z., Greene, M. I., Zhu, Z., & Zhang, H. (2020). Structural features and PF4 functions that occur in heparin-induced thrombocytopenia (HIT) complicated by COVID-19. Antibodies, 9(4), 1-17. https://doi.org/10.3390/antib9040052

[16] Heestermans, M., Poenou, G., Hamzeh-Cognasse, H., Cognasse, F., & Bertoletti, L. (2022). Anticoagulants: A Short History, Their Mechanism of Action, Pharmacology, and Indications. Cells, 11(20), 1-17. https://doi.org/10.3390/cells11203214

[17] Ito, D., Ge, D., Kogure, N., Manaka, H., Terui, Y., Takayama, H., Linhardt, R. J., Toida, T., & Higashi, K. (2020). Poly-ion complex (PIC) formation of heparin and polyamines: PIC with tetrakis (3-aminopropyl) ammonium allows sustained release of heparin. Heliyon, 6(10), e05168. https://doi.org/10.1016/j.heliyon.2020.e05168

[18] Pant, B., Park, M., & Park, S. J. (2019). Drug delivery applications of core-sheath nanofibers prepared by coaxial electrospinning: A review. Pharmaceutics, 11(7). https://doi.org/10.3390/pharmaceutics11070305

[19] Orozco, P., Montoya, Y., García-García, A., & Bustamante, J. (2025). Physical and chemical effect of an electrospun nanocomposite of gelatin/polyvinyl alcohol loaded with heparin. Results in Materials, 26. https://doi.org/10.1016/j.rinma.2025.100703

[20] Soliman, S., Sant, S., Nichol, J. W., Khabiry, M., Traversa, E., & Khademhosseini, A. (2011). Controlling the porosity of fibrous scaffolds by modulating the fiber diameter and packing density. Journal of Biomedical Materials Research - Part A, 96 A(3), 566-574. https://doi.org/10.1002/jbm.a.33010

[21] Wang, X., Lou, T., Zhao, W., Song, G., Li, C., & Cui, G. (2016). The effect of fiber size and pore size on cell proliferation and infiltration in PLLA scaffolds on bone tissue engineering. Journal of Biomaterials Applications, 30(10), 1545-1551. https://doi.org/10.1177/0885328216636320

[22] Areias, A. C., Ribeiro, C., Sencadas, V., Garcia-Giralt, N., Diez-Perez, A., Gómez Ribelles, J. L., & Lanceros-Méndez, S. (2012). Influence of crystallinity and fiber orientation on hydrophobicity and biological response of poly(l-lactide) electrospun mats. Soft Matter, 8(21), 5818-5825. https://doi.org/10.1039/c2sm25557j

[23] Moreno Raja, M., Lim, P. Q., Wong, Y. S., Xiong, G. M., Zhang, Y., Venkatraman, S., & Huang, Y. (2019). Polymeric Nanomaterials. In Nanocarriers for Drug Delivery. Elsevier Inc. https://doi.org/10.1016/b978-0-12-814033-8.00018-7

[24] Kim, C. H., Khil, M. S., Kim, H. Y., Lee, H. U., & Jahng, K. Y. (2006). An improved hydrophilicity via electrospinning for enhanced cell attachment and proliferation. Journal of Biomedical Materials Research - Part B Applied Biomaterials, 78(2), 283-290. https://doi.org/10.1002/jbm.b.30484

[25] Rodríguez-Soto, M. A., Polanía-Sandoval, C. A., Aragón-Rivera, A. M., Buitrago, D., Ayala-Velásquez, M., Velandia-Sánchez, A., Peralta Peluffo, G., Cruz, J. C., Muñoz Camargo, C., Camacho-Mackenzie, J., & Barrera-Carvajal, J. G. (2022). Small Diameter Cell-Free Tissue-Engineered Vascular Grafts: Biomaterials and Manufacture Techniques to Reach Suitable. Polymers, 14(3440).

[26] Rwei, S. P., & Huang, C. C. (2012). Electrospinning PVA solution-rheology and morphology analyses. Fibers and Polymers, 13(1), 44-50. https://doi.org/10.1007/s12221-012-0044-9

[27] Yang, H., Zhu, G., Zhang, Z., Wang, Z., Fang, J., & Xu, W. (2012). Influence of weft-knitted tubular fabric on radial mechanical property of coaxial three-layer small-diameter vascular graft. Journal of Biomedical Materials Research - Part B Applied Biomaterials, 100 B(2), 342-349. https://doi.org/10.1002/jbm.b.31955

[28] Li, M. X., Li, L., Zhou, S. Y., Cao, J. H., Liang, W. H., Tian, Y., Shi, X. T., Yang, X. Bin, & Wu, D. Y. (2021). A biomimetic orthogonal-bilayer tubular scaffold for the co-culture of endothelial cells and smooth muscle cells. RSC Advances, 11(50), 31783-31790. https://doi.org/10.1039/d1ra04472a

Contribution of Individual Authors to the Creation of a Scientific Article (Ghostwriting Policy)

The authors contributed in the present research, at all stages from the formulation of the problem to the final findings and solution.

Sources of Funding for Research Presented in a Scientific Article or Scientific Article Itself

This study is supported by the TUSEB Project under grant no. 46602, and ITU Scientific Research Projects Unit, project number MDK-2025-46820.

Conflict of Interest

The authors have no conflicts of interest to declare that are relevant to the content of this article.